Supplement of Geosci. Model Dev., 17, 881–898, 2024
https://doi.org/10.5194/gmd-17-881-2024-supplement

Geoscientific Model Development
Open Access
EGU

Supplement of

P3D-BRNS v1.0.0: a three-dimensional, multiphase, multicomponent, pore-scale reactive transport modelling package for simulating biogeochemical processes in subsurface environments

Amir Golparvar et al.

Correspondence to: Amir Golparvar (amir.golparvar@physik.hu-berlin.de)

Outline:

This document contains:

- Section S.1: Derivation of the global indicator function
- Section S.2: Analytical solution for mass transfer across fluid-fluid interface
- Section S.3: Results obtained with P3D-BRNS from denitrification scenario that are not included in the main manuscript
- Section S.4: 3D visualizations for section 3.4 - explanation of the video supplements

S.1 Derivation of the global indicator function

A common misconception about the compressive velocity factor in equation 7 (of the main manuscript) is that it is rather considered an artificially added parameter than a derived one. In order to derive a global indicator function, we first start by writing mass conservation for the indicator function in aqueous and gaseous phase separately:

$$\begin{aligned} &\frac{\partial \alpha}{\partial t} + \nabla \cdot (\alpha \overline{\boldsymbol{u}}_{\alpha}) = 0 \qquad in\ \Omega_{\vartheta,aq} \\ &\frac{\partial \beta}{\partial t} + \nabla \cdot \left(\beta \overline{\boldsymbol{u}}_{\beta}\right) = 0 \qquad in\ \Omega_{\vartheta,gs} \end{aligned} \tag{1}$$

$\overline{\boldsymbol{u}}_{\alpha}$ and $\overline{\boldsymbol{u}}_{\beta}$ are the average velocities in aqueous and gaseous phases respectively. Recalling $\alpha + \beta = 1$ and that we solve for global velocity ($\overline{\boldsymbol{u}}$) rather than phase velocity ($\overline{\boldsymbol{u}}_{\alpha,\beta}$), equation (1) can be further developed as:

$$\begin{aligned} \frac{\partial \alpha}{\partial t} + \nabla \cdot (\alpha \overline{\boldsymbol{u}}_{\alpha}) &= \frac{\partial \alpha}{\partial t} + \nabla \cdot (\alpha(\alpha + \beta)\overline{\boldsymbol{u}}_{\alpha}) \\ &= \frac{\partial \alpha}{\partial t} + \nabla \cdot (\alpha\alpha \overline{\boldsymbol{u}}_{\alpha}) + \nabla \cdot (\alpha\beta \overline{\boldsymbol{u}}_{\alpha}) \\ &= \frac{\partial \alpha}{\partial t} + \nabla \cdot (\alpha\alpha \overline{\boldsymbol{u}}_{\alpha}) + \nabla \cdot (\alpha\beta \overline{\boldsymbol{u}}_{\alpha}) + \left(\nabla \cdot \left(\alpha\beta \overline{\boldsymbol{u}}_{\beta}\right) - \nabla \cdot \left(\alpha\beta \overline{\boldsymbol{u}}_{\beta}\right)\right) \\ &= \frac{\partial \alpha}{\partial t} + \nabla \cdot \left(\alpha\left(\alpha \overline{\boldsymbol{u}}_{\alpha} + \beta \overline{\boldsymbol{u}}_{\beta}\right)\right) + \nabla \cdot \left(\alpha\beta\left(\overline{\boldsymbol{u}}_{\alpha} - \overline{\boldsymbol{u}}_{\beta}\right)\right) \end{aligned} \tag{2}$$

$$= \frac{\partial \alpha}{\partial t} + \nabla \cdot (\alpha \bar{\boldsymbol{u}}) + \nabla \cdot (\alpha \beta \boldsymbol{u_c})$$

with $\boldsymbol{u_c} = \bar{\boldsymbol{u}}_\alpha - \bar{\boldsymbol{u}}_\beta$. The latter term in equation (2) is only nonzero if (in a given computational cell,) both phases are present, and it vanishes if the computational cell lies within aqueous (i.e. $\alpha = 1, \beta = 0$) or gaseous (i.e. $\alpha = 0, \beta = 1$) phase.

S.2 Analytical solution for mass transfer across fluid-fluid interface

We look for a 1D solution of the transient, pure diffusive mass flux problem given by a set of equations in eq. 25 of the main manuscript. The tube is considered infinite because of the free outlet left and right boundaries which is a fair assumption as we only look at the concentration profile of the tracer in early times from the start of the simulation. The tracer concentration in the entire domain can be calculated as (Bird, 2002):

$$C_{tr}^{t}(x) = \begin{cases} C_{tr,aq}^{t=0} + \dfrac{\left(C_{tr,gs}^{t=0} - H C_{tr,aq}^{t=0}\right)}{H + \sqrt{\dfrac{D_{tr,aq}}{D_{tr,gs}}}} \left(1 + erf\left(\dfrac{x}{\sqrt{4 D_{tr,aq} t}}\right)\right), & 0 < x < 0.005 \\ C_{tr,gs}^{t=0} + \dfrac{\left(C_{tr,aq}^{t=0} - \dfrac{1}{H} C_{tr,gs}^{t=0}\right)}{\dfrac{1}{H} + \sqrt{\dfrac{D_{tr,gs}}{D_{tr,aq}}}} \left(1 - erf\left(\dfrac{x}{\sqrt{4 D_{tr,gs} t}}\right)\right), & 0.005 < x < 0.01 \end{cases} \quad (3)$$

with having x as the position (in meters), $C_{tr,it=0}$ as the initial concentration of the tracer in the ith phase, t as the time (in seconds), H as the Henry's constant and Dtr,i as the diffusion coefficient of the tracer in the ith phase. **Figure S.1** shows the comparison between the analytical solution and the numerical simulation. As expected, the concentration jump at the interface is always satisfied. Moreover, we observe a very good agreement between simulation and analytical results which validates the implementation of the concentration equation for multiphase systems.

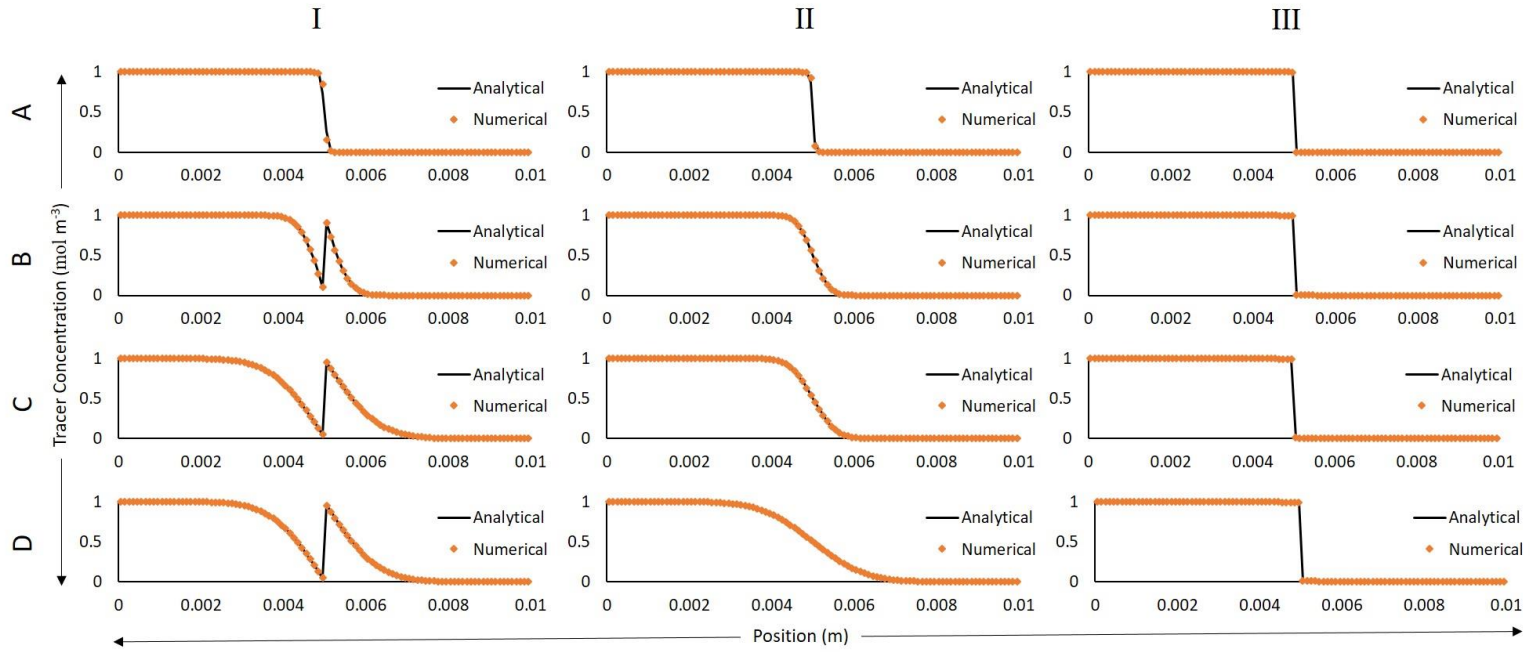

Figure S.1: Concentration profile of a volatile tracer in the entire one-dimensional domain. Each column represents cases with different values of Henry's constant and each row shows the evolution of the tracer concentration field with respect to time. Cases I, II and III have the *H-value* of 100, 1 and 0.01 respectively. A, B, C and D represent the time at 0.0001s, 0.005s, 0.01s and 0.05s respectively. For the case with high Henry's constant, the tracer becomes more volatile, and tends to cross the interface more freely compared to the other scenarios.

S.3 Results obtained with P3D-BRNS from denitrification scenario that are not included in the main manuscript

To have a better grasp of flow type and possible channelling in the porous domain, we have calculated the residence time distribution (RTD) for a non-reactive tracer with three different Henry's coefficient ($H_l = 0.01, H_m = 1, H_h = 100$) but similar diffusivity to that of oxygen. Table S.1 summarizes the parameters and their corresponding values used for this simulation (the diffusivity coefficients are shown in pairs; the first and second values denote diffusion in water and in the air, respectively). The flux weighted average of both oxygen and tracer concentration are obtained at the outlet (i.e. bottom part of the domain). Finally the RTD for each component is numerically computed from the following equation:

$$\mathrm{E(t)} = \frac{d}{dt}\left(\frac{C_{tracer}^{outlet}(t)}{C_{tracer}^{inlet}(t=0)}\right) \tag{44}$$

Residence time distribution for the three different sets of tracer simulations, along with the RTD of oxygen from the reactive transport scenario are plotted in **Error! Reference source not found.**. Assuming having a homogeneous porous system, for a pure-diffusion scenario of an inert tracer with diffusion coefficient of 2e-6 m^2 s^{-1} (corresponding to diffusivity of a chemical specie in the air – see Table S.1) the breakthrough time is expected to be $t_{bt} = \frac{(length\ of\ the\ porous\ medium)^2}{\sqrt{4(diffusion\ coefficient)}} = \frac{0.000601^2}{\sqrt{4\times 0.000002}} = 0.04\ s$. Since the advective transport is also present in all of the simulations, the expected breakthrough time is expected to be lower than the calculated t_{bt}. Hence the RTD graphs are shown for 0.1s. RTD of oxygen is comparable to that of a tracer with high *H-value*. The difference arise from the biochemical reactions that oxygen is involved in which has resulted in an apparent shorter stay of oxygen in the domain. Comparing the graphs for the three tracers suggest that under the conditions applied here, adding a surfactant which results in decreasing Henry's constant (i.e. decreasing volatility), can help with keeping chemical species longer in the domain. In a broader sense, our model is best suitable for parametric study to identify the relevant and/or dominant factors that shape the fate of chemicals in porous media, and hence developing an optimum operating strategy to have the best favourable outcome.

Table S.1: Model parameters

Parameters	Value	Unit
μ_{max}	0.066^{*}	$(mol\ suc.)(C-mol\ biomass)^{-1}h^{-1}$
K_{O_2}	8.28^{*}	μM
K_{I,NO,O_2}	0.0174^{*}	μM
K_{NO_3}	13000^{*}	μM
$K_{I,O_2,NAP}$	4^{*}	μM
$nNAP$ (exponent)	4^{*}	$-$
K_{NO_2}	880^{*}	μM
$K_{I,O_2,NIR}$	3.58^{*}	μM
$nNIR$ (exponent)	3.7^{*}	$-$
K_{NO}	0.0081^{*}	μM
$K_{I,O_2,NOR}$	1.0^{*}	μM
$K_{I,NO}$	20^{*}	μM
$\upsilon_{m,NAP}$	0.0667^{*}	h^{-1}
$K_{NO_3,NAP}$	0.00001^{*}	μM
$\upsilon_{m,NIR}$	0.0667^{*}	h^{-1}
$K_{NO_2,NIR}$	50^{*}	μM
$\upsilon_{m,NOR}$	1^{*}	h^{-1}
$K_{NO,NOR}$	0.054^{*}	μM
$K_{O_2,NOR}$	400^{*}	μM
H_{O_2}	31^{*}	$-$
H_{NO}	21^{*}	$-$
H_{N_2O}	1.74^{*}	$-$
H_{NO_2}	2.88^{*}	$-$
H_{NO_3}	1.06^{*}	$-$
H_{suc}	10^{-4}	$-$
$D_{O_2}(aq,air)$	$(2\times10^{-9}, 2\times10^{-5})^{**}$	$m^2\ s^{-1}$
$D_{NO}(aq,air)$	$(1\times10^{-9}, 2\times10^{-6})^{**}$	$m^2\ s^{-1}$
$D_{N_2O}(aq,air)$	$(1\times10^{-9}, 2\times10^{-6})^{**}$	$m^2\ s^{-1}$
$D_{NO_2}(aq,air)$	$(2\times10^{-9}, 2\times10^{-6})^{**}$	$m^2\ s^{-1}$

$D_{NO_3}(aq, air)$	$(2 \times 10^{-9}, 2 \times 10^{-6})^{**}$	$m^2\ s^{-1}$
$D_{suc}(aq, air)$	$(1 \times 10^{-9}, 2 \times 10^{-15})^{**}$	$m^2\ s^{-1}$

*The values are extracted from (Kampschreur et al., 2012).

**The values are obtained from Phreeqc (Parkhurst and Appelo, 1999).

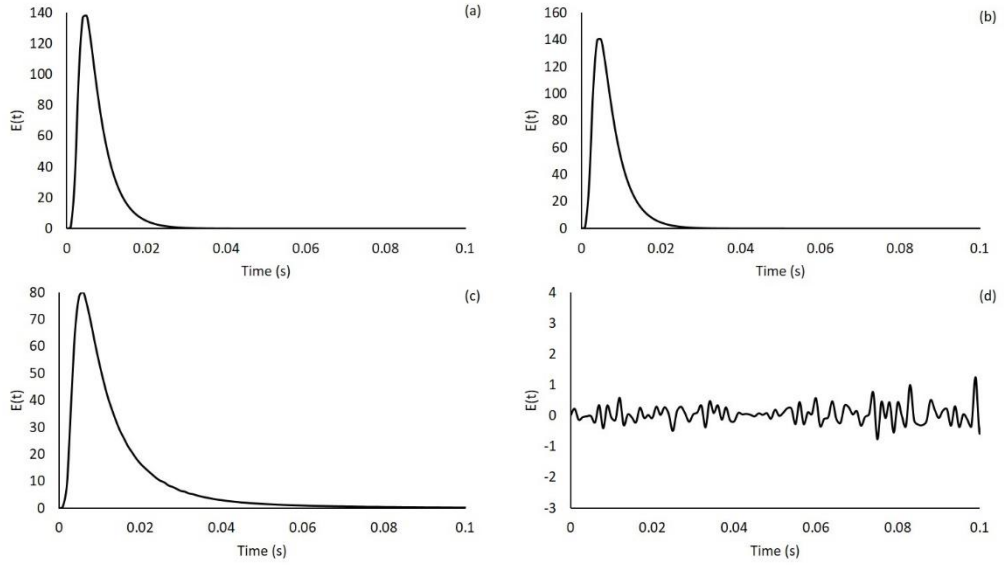

Figure S.2: Residence time distribution for 1) the reactive oxygen from the denitrification simulation (a) and 2) an inert tracer with high (b), mid (c) and low (c) values of Henry's constant.

S.4 3D visualizations: explanation of the video supplements

Post-processing native OpenFoam applications are viable using Paraview (Ahrens et al., 2005). Paraview provides all the necessary tools to visualize the µ-CT images and analyse all minds of data types produced by OpenFOAM (Greenshields, 2015). To have a better grasp of the physical domain studied in section 3.4 of the main article (i.e. denitrification scenario), the overall architecture of the 3D porous material and distribution of different phases/species, the numerical results are interpreted in Paraview as follows (Golparvar et al., 2022):

1. "Supp-1.mpg" shows the 3D structure of the porous material,
2. "Supp-2.mpg" and "Supp-3.mpg" illustrate the steady-state distribution of water and air in the pore volume, respectively,

3. Succinate and Oxygen distributions in the domain can be found in “Supp-4.mpg” and “Supp-5.mpg” respectively.

References

Ahrens, J., Geveci, B., and Law, C.: Paraview: An end-user tool for large data visualization, The visualization handbook, 717, 2005.

Bird, R. B.: Transport phenomena, Appl. Mech. Rev., 55, R1-R4, 2002.

Golparvar, A., Kaestner, M. and Thullner, M.: Movies, , doi:10.6084/m9.figshare.19391405.v2, 2022.

Greenshields, C. J.: OpenFOAM user guide, OpenFOAM Foundation Ltd, version, 3, 47, 2015.

Kampschreur, M. J., Kleerebezem, R., Picioreanu, C., Bakken, L. R., Bergaust, L., de Vries, S., Jetten, M. S., and Van Loosdrecht, M.: Metabolic modeling of denitrification in Agrobacterium tumefaciens: a tool to study inhibiting and activating compounds for the denitrification pathway, Frontiers in microbiology, 3, 370, 2012.

Parkhurst, D. L., and Appelo, C. A. J.: User's guide to PHREEQC (Version 2) : a computer program for speciation, batch-reaction, one-dimensional transport, and inverse geochemical calculations, Report 99-4259, 1999.